9 March 2001

ELSEVIER

Chemical Physics Letters 336 (2001) 88–96

CHEMICAL PHYSICS LETTERS

www.elsevier.nl/locate/cplett

Three-dimensional imaging of orientational order by fluorescence confocal polarizing microscopy

I.I. Smalyukh, S.V. Shiyanovskii, O.D. Lavrentovich *

Chemical Physics Interdisciplinary Program and Liquid Crystal Institute, Kent State University, Kent, OH 44242, USA

Received 15 September 2000

Abstract

We develop the technique of fluorescence confocal polarizing microscopy to image three-dimensional patterns of orientational order. The method employs the property of anisometric fluorescent dye molecules to orient in an anisotropic medium. When the confocal observation is performed in polarized light, the detected fluorescence signal is determined by the orientation of the molecules. The technique literally adds a new dimension to the studies of the ordered media such as liquid crystals by revealing how the orientation of molecules changes not only in the plane of observations, but also along the direction of observation.

1. Introduction

Orientational order is a universal feature of numerous soft-matter systems of physical, chemical, and biological significance [1]. These systems have partial or no positional order and are extremely flexible, producing a rich variety of complex three-dimensional (3D) spatial patterns. Non-destructive techniques to study these patterns are in a great demand. Most of the available techniques, such as nuclear magnetic resonance, X-ray diffraction, optical polarizing microscopy (PM), produce only an integrated image of the 3D structure. For example, PM tests orientation of the optic axes that are closely related to the structure of the medium [2–4]. However, a PM image bears only a two-dimensional (2D) information, integrating the 3D pattern of optical birefringence over the path of light [4]. On the other hand, the fluorescence confocal microscopy (FCM) successfully images the 3D systems with spatially varied density and composition [5,6], including individual molecules [7]. In this work, we demonstrate that the polarized light FCM can be used to image 3D patterns of the orientational (rather than positional) order. As an example we visualize 3D structures in the lamellar (smectic A) and nematic (N) liquid crystals. The N liquid crystal is a classical example of the orientationally ordered soft-matter medium: the molecules are on average parallel to some axis called the director $\hat{\mathbf{n}}$. In smectic A (SmA) this orientational order is accompanied by a partial one-dimensional positional order, as the molecules form layers perpendicular to $\hat{\mathbf{n}}$. The in situ fluorescence confocal polarizing microscopy (FCPM) observation reveals the orientational pattern of $\hat{\mathbf{n}}$ both in the plane of observation and perpendicular to it; the later feature is an important advantage over other non-destructive imaging techniques such as PM.

* Corresponding author. Fax: +1-330-672-2796.
E-mail address: odl@lci.kent.edu (O.D. Lavrentovich).

0009-2614/01/$ - see front matter
PII: S0009-2614(00)01471-8

2. Experimental

The principal scheme of the FCPM technique is shown in Fig. 1. The studied material is doped with a fluorescent dye. We used a fluorescent dye *n*, *n*′-*bis*(2,5-di-tert-butylphenyl)-3,4,9,10-perylenedicarboximide (BTBP), Fig. 2a, with maximum absorption for light polarization along the long axis of the molecule [8]. The BTBP dye was added in tiny quantities of 0.01% (by weight), well below the solubility limits, to two materials: a SmA single-component material 4′-*trans*-butyl-4-cyano-4-*trans*-heptyl-1,1′-bicyclohexane (CCN-47), Fig. 2b, and a nematic mixture ZLI-3412. Both liquid crystals have low birefringence: the difference between the extraordinary and ordinary refractive indices is ≈ 0.07 for the nematic ZLI-3412, and ≈ 0.04 for CCN-47. We used Olympus Fluoview BX-50 confocal microscope, modified by a linear polarizer **P** that sets polarization $\mathbf{P}_e||\mathbf{P}$ of the excitation beam and the polarization $\mathbf{P}_f||\mathbf{P}$ of the detected fluorescent light (Fig. 1). The excitation beam (488 nm, Ar laser) is focused by an objective into a small (<1 μm^3) volume in the cell. The

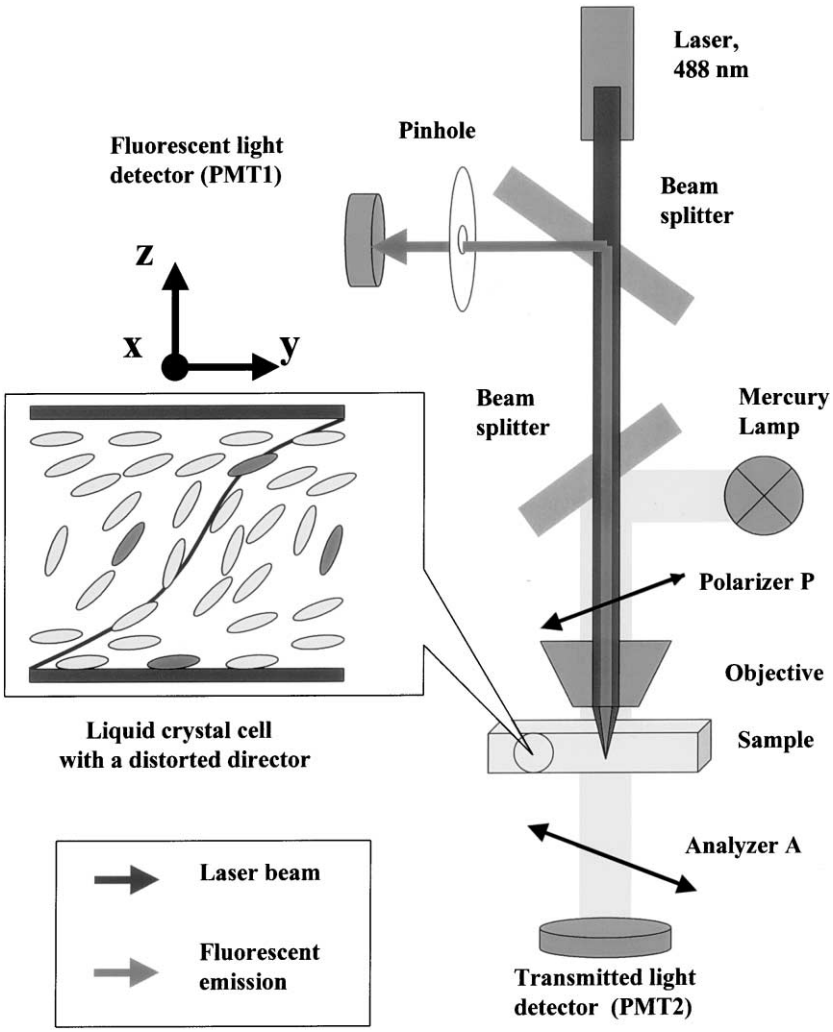

Fig. 1. Scheme of FCPM (see text).

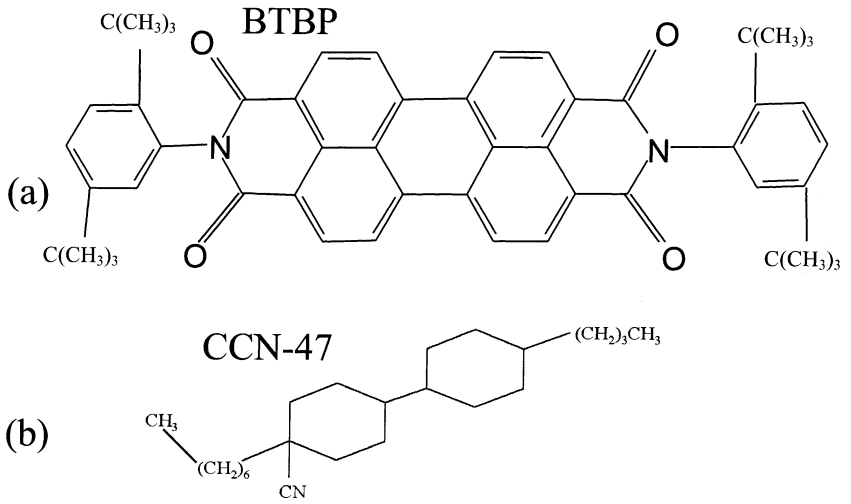

Fig. 2. Molecular structures of fluorescent BTBP (a) and SmA material CCN-47 (b).

fluorescent light from this volume is detected by a photomultiplier tube (PMT1) in the spectral region 510–550 nm. A 100 μm wide pinhole discriminates against the regions above and below the selected volume [5,6]. The beam power is small, ~120 nW, to avoid light-induced reorientation of the dye-doped liquid crystal. To verify if the dye is well oriented, we prepared a nematic cell with $\hat{\mathbf{n}}$ aligned uniformly in the plane of the cell, and measured the intensity of fluorescence (averaged over the cell area) as the function of the angle between **P** and $\hat{\mathbf{n}}$. The intensity of fluorescence is maximum when $\mathbf{P}||\hat{\mathbf{n}}$ and minimum when $\mathbf{P} \perp \hat{\mathbf{n}}$, the ratio being 7.5, which indicates that the dye molecules are well oriented along $\hat{\mathbf{n}}$. The strong orientation dependence of measured fluorescence signal allows one to decipher the 3D orientation pattern from the FCPM observations.

The focused beam scans the sample both in the horizontal plane, located at a fixed depth z, and in the vertical plane. The intensity of fluorescence is measured and stored in the computer memory, as a thin 'optical slice' [5]. The thickness of the slice is defined by the resolution of the FCPM. The resolution is about 1 μm for slabs of small birefringence and thickness 20 μm or less.

Simultaneously with the FCPM image, a usual transmitted PM texture of the same sample is recorded by measuring the intensity of light (spectral region 585–610 nm, PMT2) that passes through the polarizer P, sample, and a crossed analyzer A, Fig. 1.

3. Results

3.1. FCPM of focal conic domains

Lamellar phases such as SmA often organize in distorted focal conic domains (FCDs) structures in which the molecular layers are bent but remain parallel to each other [9]. The layers adopt the shape of Dupin cyclides, i.e., surfaces whose lines of curvature are circles. A family of Dupin cyclides is associated with a pair of confocal hyperbola and ellipse, located in the two mutually perpendicular planes [9]. The layers fold around the pair in such a way that they remain everywhere perpendicular to the straight lines that connect any point on the ellipse to any point on the hyperbola, Fig. 3a. These straight lines are simultaneously the director and local optical axes [2,9], Fig. 3b–d.

To produce and observe the FCDs, we assembled SmA cells with two transparent and electroconductive plates treated by lecithin for normal surface orientation of the director. The thickness of the SmA slab is $d = 20$ μm. The sample with $\hat{\mathbf{n}}$ perpendicular to the plates ($n_x = 0,\ n_y = 0,\ n_z = 1$)

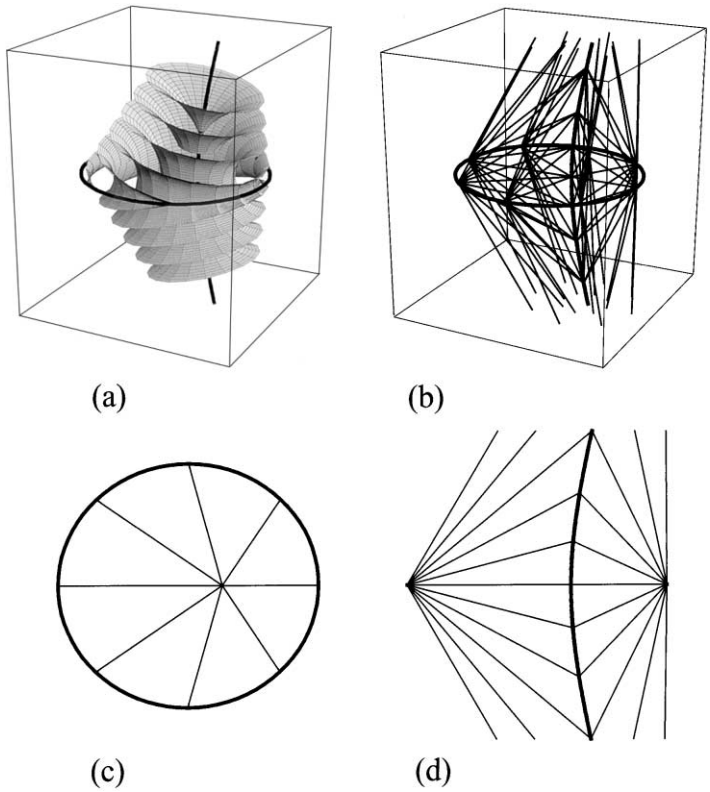

Fig. 3. FCD in a Sm A liquid crystal: (a) layers curved around the confocal ellipse and hyperbola; (b) a corresponding 3D pattern of the director field; (c) cuts of the director field by a horizontal plane that contains the ellipse; (d) a vertical plane that contains the hyperbola.

shows extinction, both in the PM mode (only ordinary wave propagates) and in the FCPM mode (as $\hat{\mathbf{n}} \perp \mathbf{P}$). An applied electric voltage produces numerous FCDs [10] of the type shown in Fig. 3. The voltage is switched off and the texture slowly (days) relaxed. Fig. 4 compares the textures of the same three FCDs when viewed by FCPM (a,b,c) and by PM (d,e,f).

FCPM textures in Fig. 4a and c are (x,y) optical slices of thickness $z_2 - z_1 \approx 1$ μm taken from the middle-plane of the cell $(z_1 + z_2)/2 \approx d/2$. This plane contains the elliptical bases of FCDs. The maximum intensity of the fluorescent light is in the regions where $\hat{\mathbf{n}}||\mathbf{P}$. Rotating the polarizer (compare 4a and 4c) we reconstruct the whole director pattern in the plane of the ellipse, which coincides with that shown in Fig. 3c. The optical information from the regions $0 < z < z_1$ and $z_2 < z < d$ is cut-off by the pinhole. This cut-off feature enables us to visualize clearly the intersection of the hyperbola defect with the plane of view as a spot (marked h in Fig. 4a) of relatively low intensity.

The standard PM textures of FCDs, Fig. 4d and f, show extinction whenever $\hat{\mathbf{n}}$ (= optical axis) is along the polarizer *or* the analyzer [2,4]. The maximum intensity is achieved for intermediate orientations. Interchanging the directions of the polarizer and the analyzer leaves the optical texture intact, Fig. 4d and f. Therefore, the standard PM does not distinguish between two mutually perpendicular director fields, while the FCPM does. However, the most striking evidence of the superiority of FCPM over PM is in the ability to resolve the structural features along the direction of view, as discussed below.

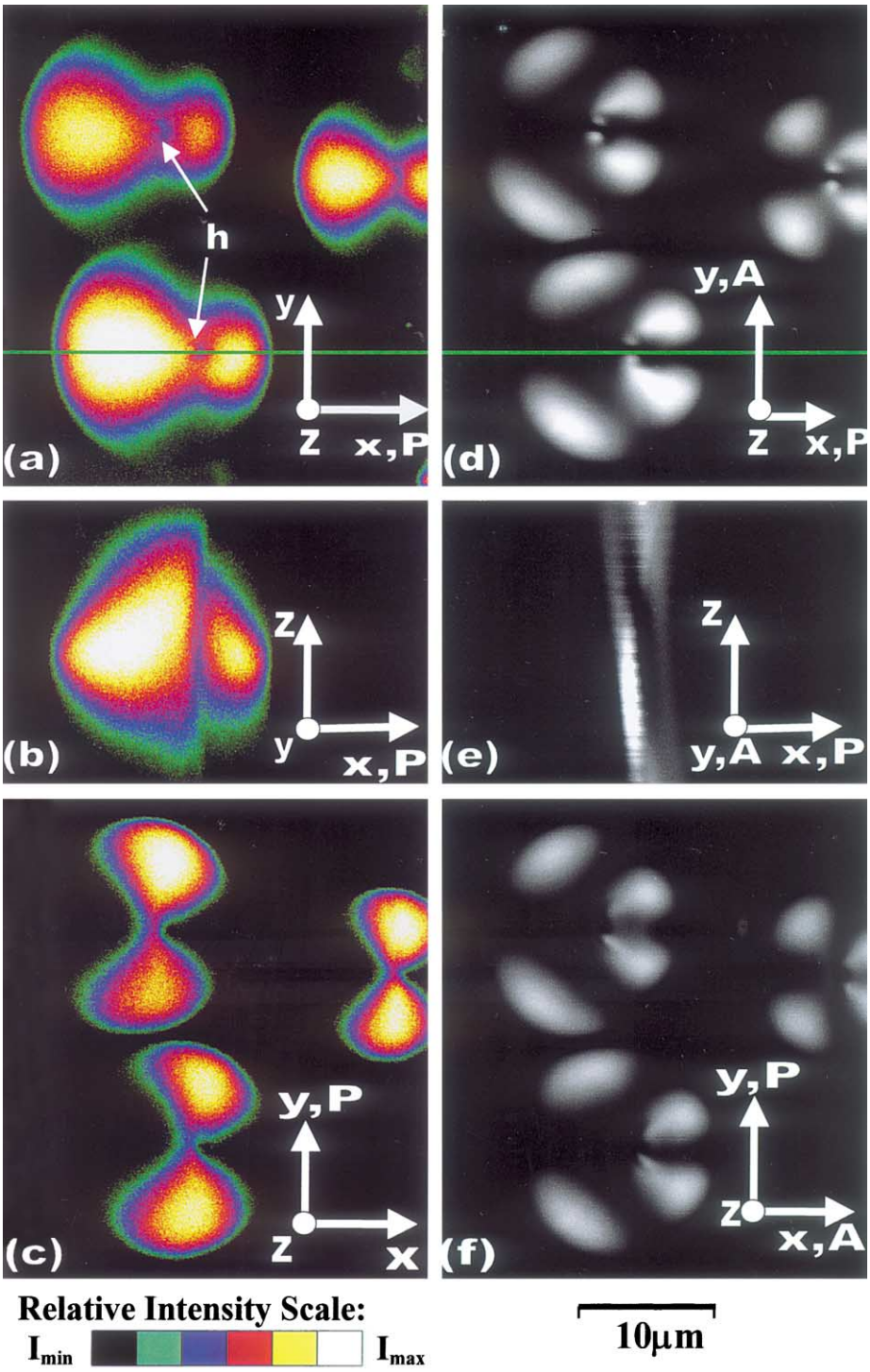

Fig. 4. Images of FCDs obtained by FCPM (a)–(c) and PM (d)–(f). Parts (a), (c), (d), and (f) are horizontal textures, while parts (b) and (e) are vertical cross-sections, see text for details. The cross-sections (b) and (e) were obtained from the vertical scan along the green lines on the parts (a) and (d), respectively.

In FCPM, refocusing the microscope at different depths z in the specimen, one obtains a vertical cross-section, assembled from many (150 in our case) horizontal slices, Fig. 4b. The maximum intensity is again in the regions, where $\hat{\mathbf{n}}||\mathbf{P}$. In particular, the surrounding of the FCD is dark, which corresponds to the director oriented along the vertical axis z. In other words, the smectic layers are parallel to the plates far away from the FCDs, as expected [9,10]. The hyperbola defect in Fig. 4b is seen as a relatively dark line, see also Fig. 3d. One would expect that at the core of the defect the liquid crystal and dye molecules are oriented along the hyperbola; since the hyperbola is almost vertical, the intensity of fluorescence should be small. Fig. 4b also demonstrates that the ellipse plane is in the middle of the cell. The reason is most probably related to the surface anchoring phenomena at the bounding plates [10]. The smectic layers cross the ellipse plane perpendicularly, Fig. 3a. If the ellipse were located at the boundary, this orientation of layers would strongly contradict the normal surface anchoring of the director [10]. When the elliptic base shifts towards the middle of the cell, the director at the surface becomes closer to vertical orientation.

Note that there is no perfect symmetry between the top and the bottom halves of the (z,x) slice in Fig. 4b. The reason is finite absorption of light (that impinges onto the top plate) by the dye-doped material, and defocusing effect that increases with the depth of scanning.

In principle, a standard PM also allows one to refocus at different depth in the sample and to measure the intensity of light that passes through the sample and the pair of polarizers, Fig. 4e. Unlike in the FCPM, however, each PM image contains information from the regions far below and above the plane of focus. The position of the elliptical base of the FCD cannot be resolved in Fig. 4e. Poor resolution in the direction of light propagation is an intrinsic problem of PM. The incident light splits into the ordinary and extraordinary waves with mutually perpendicular polarizations and amplitudes that depend on the director orientation and the polarization of incident light. The phase difference between the two waves at the exit of the sample is converted into the intensity pattern by the analyzer. Thus, as explained in detail by Bellare et al. [4], the information about the z-variations is compressed to the integral of the certain component of the local dielectric tensor, related to the directions of the polarizer and the analyzer. Computer simulation [4] reveal, for example that the PM images of FCDs are hard to distinguish from the images of other objects with completely different geometry, for example, fused spheres, even when the observations are made for different directions of view. In contrast, the FCPM images in Fig. 4a–c are unambiguously those of FCDs.

The experiments described above and in Fig. 4 refer to the thermotropic SmA. We also succeeded in FCPM imaging of structures in the lyotropic counterpart of SmA, the L_α lamellar phase formed by the mixture of cetylpyridinium chloride, hexanol, and brine [11].

3.2. FCPM of Frederiks transition

Now we turn to the classic Frederiks effect in the N liquid crystal, to demonstrate that the FCPM can be employed successfully to the studies of electro-optic effects that are at the heart of numerous applications of liquid crystals [12].

The nematic slab (thickness 20 μm) was prepared between two transparent electroconductive plates coated with a rubbed polyimide PI2555 to provide a planar structure ($\hat{\mathbf{n}}$ is parallel to the axis y, Fig. 5). The electric ac voltage is applied between the plates. Since ZLI-3412 has a positive dielectric anisotropy, the applied field tends to reorient the director vertically. At small voltages, the structure remains uniform, $n_x = 0$, $n_y = 1$, $n_z = 0$ (Fig. 5a). Above a well-defined threshold of 2.6 V, the electric field reorients $\hat{\mathbf{n}}$ from its strictly horizontal orientation towards the z-axis [12]. In the FCPM textures the transition is manifested by the reduced intensity of fluorescent light. Note that the bands of low intensity in Fig. 5a are located in the middle of the cell. This is precisely what the theory of Frederiks transition predicts [12]: the maximum deviation of $\hat{\mathbf{n}}$ should be in the middle-plane, Fig. 5b. As the field increases, both the amplitude of the director reorientation and the thickness of the reoriented zone should increase,

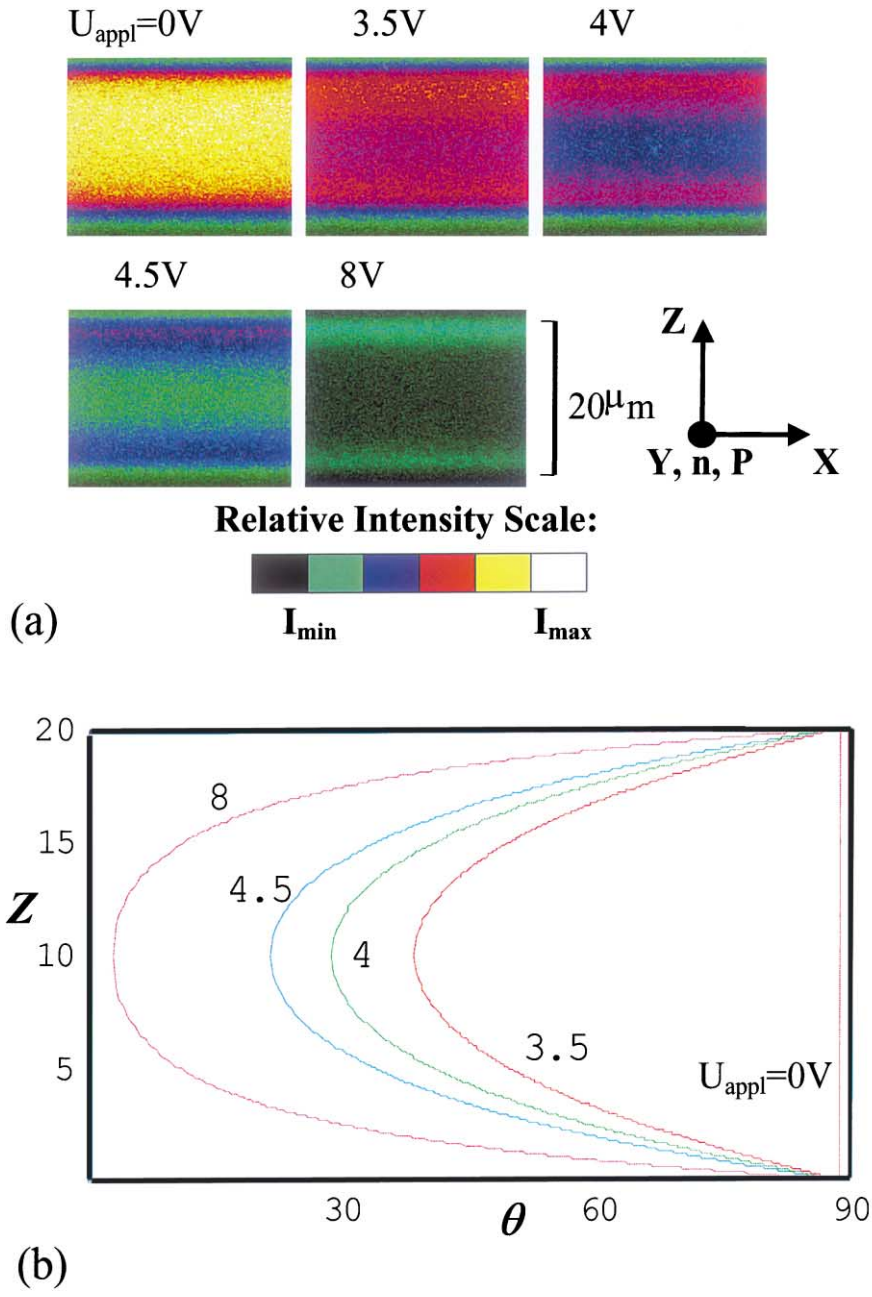

Fig. 5. FCPM textures of the vertical cross-sections (a) and computer simulations of the angle θ between the director and the surface normal (b) in a nematic sample undergoing Frederiks transition.

Fig. 5b. This prediction of the theory is clearly visualized in the FCPM images of the vertical cross-section of the cell, Fig. 5a. Note that the director pattern and its evolution in the vertical cross-section of the cell cannot be obtained with PM.

4. Discussion

Most of the applications of FCM in biology and materials science employ the spatial variation of dye concentration across the sample to achieve the optical contrast, see, e.g. [13–16]. The fluorophores can selectively tag the component of interest in mixtures, for example, a polymer in a phase separating monomer–liquid crystal mixture; the fluorescent polymer network then reveals the orientation of the surrounding liquid crystal [15]. The confocal microscope, even in the non-polarized mode, can also image director patterns in samples with no phase separation, e.g., in cholesteric 'fingerprint' textures [17,18]. However, in the fingerprint textures the director changes predominantly in the plane of the sample and little along the z-axis; the advantage of FCPM over PM is hard to see. In contrast, the two examples presented in this work have the director field markedly z-dependent. For this general case, the FCPM technique is by far superior than its regular PM counterpart. The contrast in our examples is related to the orientation of the fluorescent probe rather than to its concentration gradients.

Practical application of FCPM requires some care to avoid aberrations and other side effects. There are issues of common importance for both optically isotropic and anisotropic media (role of the bounding plates, photobleaching, etc., see, e.g. [19]). Below we list some of the issues specific for FCPM of anisotropic media.

(1) *Fluorescent probe*. The probe should dissolve, align and fluoresce in the anisotropic host. Different materials (e.g., thermotropic vs lyotropic liquid crystals) would require different dyes. To study electro-optic phenomena, especially in dc fields, one might wish to avoid dyes of ionic nature as these would redistribute in the electric field; the intensity pattern might reflect the non-uniform concentration of the ionic dye rather than the director orientation. The concentration of dye and the intensity of light should be low enough to avoid light-induced director distortions in dye-doped liquid crystals [20].

(2) *Optics of anisotropic medium*. Focusing the laser beam in a birefringent medium is more complicated than in an isotropic medium since there are two propagating modes with different indices of refraction. To reduce the aberrations one can use a liquid crystal host with a low birefringence Δn: the spatial defocusing of the two modes is $g\Delta nz/\bar{n}$, where $\bar{n}$ is the average refractive index, z is the depth of scanning, and g is a coefficient of the order of unity (dependent on the director orientation).

(3) *Light absorption*. Reducing the concentration of dye, the depth of scanning, and the thickness of the sample all help to mitigate this problem.

(4) *Adiabatic following of polarization*. The well-known effect in the optics of liquid crystals is that the polarization of both ordinary and extraordinary waves can follow the local orientation of $\hat{\mathbf{n}}$ in a twisted cell (the so-called Mauguine regime). This effect must be taken into account while interpreting the FCPM images for samples with twist deformations, especially when the twist scale is supra-micron and light propagates along the twist axis.

(5) *Polarization geometry*. We used the scheme in which the very same linear polarizer determines polarization of both the incident and the detected fluorescent light. Depending on the need, one can design many other polarization geometries.

(6) *Concentration gradients*. Even in a one-component anisotropic medium, there is a possibility that the dye concentration would be spatially non-uniform as the director gradients might cause concentration gradients of the dyes. Fortunately, for soluble dopants the effect is strong only when the scale of distortions is comparable to the molecular scale [21].

5. Conclusion

The FCPM technique proposed in this Letter is capable to image 3D patterns of orientational order. The technique is not restricted to thermotropic and lyotropic, nematic and smectic phases but is applicable whenever the host for the fluorescent probe is orientationally ordered. Important fields of applications include high-tensile strength polymers, vesicles and membranes, colloids, etc. The methodological tools of FCPM presented here

provide the basis for further expansion of the technique.

Acknowledgements

We thank J. Kelly, M. Kleman, D. Voloshchenko, and D.-K. Yang for discussions. This work was supported by NSF ALCOM Grant No. DMR89-20147.

References

[1] P.M. Chaikin, T.C. Lubensky, Principles of Condensed Matter Physics, Cambridge University Press, Cambridge, 1995.
[2] N.H. Hartshorn, The Microscopy of Liquid Crystals, Microscope Publications, London, 1974.
[3] J.M. Haudin, in: G.H. Meeten (Ed.), Optical Properties of Polymers, Elsevier, Essex, 1986, pp. 167–264.
[4] J.R. Bellare, H.T. Davis, W.G. Miller, L.E. Scriven, J. Colloid Interface Sci. 136 (1990) 305.
[5] R.H. Webb, Rep. Prog. Phys. 59 (1996) 427.
[6] J.B. Pawley (Ed.), Handbook of Biological Confocal Microscopy, second ed., Plenum Press, New York, 1995.
[7] S. Nie, D.T. Chiu, R.N. Zare, Science 266 (1994) 1018.
[8] A.J. Bur, S.C. Roth, S.C. Thomas, Rev. Sci. Instr. 71 (2000) 1516.
[9] M. Kleman, Points, Lines and Walls in Liquid Crystals, Magnetic Systems and Various Ordered Media, Wiley, Chichester, 1983.
[10] Z. Li, O.D. Lavrentovich, Phys. Rev. Lett. 73 (1994) 280.
[11] P. Boltenhagen, O. Lavrentovich, M. Kleman, J. Phys. II, France 1 (1991) 1233.
[12] L.M. Blinov, V.G. Chigrinov, Electrooptic Effects in Liquid Crystal Materials, Springer, New York, 1994.
[13] W.R. White, P. Wiltzius, Phys. Rev. Lett. 75 (1995) 3012.
[14] J. Korlach, P. Schwille, W.W. Webb, G.W. Feigenson, Proc. Natl. Acad. Sci. USA 96 (1999) 8461.
[15] G.A. Held, L.L. Kosbar, I. Dierking, A.C. Lowe, G. Grinstein, V. Lee, R.D. Miller, Phys. Rev. Lett. 79 (1997) 3443.
[16] J.B. Nephew, T.C. Nihei, S.A. Carter, Phys. Rev. Lett. 80 (1998) 3276.
[17] O.D. Lavrentovich, S.V. Shiyanovskii, D. Voloschenko, Proc. SPIE 3787 (1999) 149.
[18] D. Voloschenko, O.D. Lavrentovich, Opt. Lett. 25 (2000) 317.
[19] S. Gibson, F. Lanni, J. Opt. Soc. Am. A. 9 (1992) 154.
[20] I. Janossy, Phys. Rev. E 49 (1994) 2957.
[21] S.V. Shiyanovskii, Ju.G. Terentieva, Phys. Rev. E 49 (1994) 916.